Surface Pressure Measurements at the Tip of a Model Helicopter Rotor in Hover

T.P. Shivananda,* H.M. McMahon,† and R.B. Gray‡
Georgia Institute of Technology, Atlanta, Ga.

Detailed blade-tip surface pressure distribution data for a single-bladed model helicopter rotor in hover are presented. The pressure measurements were made along the chordwise direction at six spanwise stations outboard of the 94% radial location on the rotor blade. Data were taken at blade collective pitch angles of 0, 6.2, and 11.4 deg at Reynolds numbers (based upon rotor tip speed and chord) of 5.44×10^5 and 7.36×10^5. The points of inception of the primary vortex inferred from the pressure data agree with those noted by other investigators using surface flow visualization techniques. The presence of both a primary and a secondary vortex near the rotor tip at a pitch angle of 11.4 deg is observed. Normal and chordwise force coefficients obtained by integrating the pressure data are also presented.

Nomenclature

C = rotor blade chord
C_p = pressure coefficient $(p-p_\infty)/q$
c_c = chordwise force coefficient
c_n = normal force coefficient
p = pressure
p_∞ = ambient pressure
q = dynamic pressure based on local blade-element velocity
r = local rotor blade radius
R = rotor blade tip radius
X = chordwise distance from blade leading edge
Y = radial distance inward from blade tip
θ = blade collective pitch angle

Introduction

THE operating characteristics of rotary wing vehicles are strongly influenced by the vortex wake of the rotating blades, the dominant feature of this wake being the helical vortices which have their origin at the tips of the rotors. Rotor theory has progressed to the point where detailed knowledge of the structure of the tip vortex is needed. In a review of a recent AGARD meeting on rotary wing aerodynamics, Ham[1] pointed out the need for a better understanding of the physical processes in the formation and structure of a blade-tip vortex. Furthermore, the traditional approach of using a "tip loss factor" in helicopter performance calculations needs to be made more precise. Thus, there is a requirement for more detailed knowledge of the flowfield very near the tip of a helicopter rotor blade.

Qualitative information on the local flow directions near the rotor tip is available from flow visualization tests.[2] Other experiments on tip vortex abatement[3] and on blade-vortex interactions[4,5] have given some insight into the flow at the tip region, but these studies have dealt either with flow visualization of the tip vortex or with the measurement of unsteady pressure distributions for $r/R \leq 0.95$. There is a lack of detailed data very near the rotor tip.

Received July 1, 1977; revision received April 10, 1978. Copyright © American Institute of Aeronautics and Astronautics, Inc., 1978. All rights reserved.

Index categories: Helicopters; Propeller and Rotor Systems; Jets, Wakes, and Viscid-Inviscid Flow Interactions.

*Graduate Research Assistant, School of Aerospace Engineering.
†Professor of Aerospace Engineering. Member AIAA.
‡Regents' Professor of Aerospace Engineering. Member AIAA.

The generation of a tip vortex by a fixed wing has received considerable attention from several investigators.[6-9] Measurement of surface pressure distributions over wings with square tips has shown the presence of a primary, as well as a secondary, vortex near the tip on the top surface of a lifting wing. Some flow visualization studies also were carried out[7] to investigate the applicability of fixed-wing results to rotating wings. It was felt[7] that the location of the tip vortex is not affected by centrifugal force, so that it is possible to carry over wing tip results to the case of a hovering rotor.

The objective of the present study was to provide detailed surface pressure distribution data very near the tip of a single-blade helicopter rotor in hover, and to investigate the change in these pressures with changes in blade collective pitch angle. The results are interpreted and compared with prior results for rotors and fixed wings. Measured pressures are tabulated for use by other investigators.

Apparatus and Procedure

Apparatus

The experiments were carried out in the helicopter rotor research facility at Georgia Tech, shown in elevation in Fig. 1. The cross section of the test cell is a square. Measurements made near the rotor plane of the mean axial velocity distribution and tip vortex location and the measured rotor performance are in reasonable agreement with the results of a prescribed vortex wake analysis for an isolated rotor. This confirms that the rotor is operating in hover within the test cell with no appreciable wall effect. The test rotor had a constant chord, untwisted blade with an NACA 0012 airfoil section. The blade chord was 5 in. and the tip radius was 24 in. The outermost 1.75 in. of the blade was made of magnesium and was removable. This tip was drilled out to form six irregularly shaped cavities whose free volume varied from approximately 0.06 to 0.10 in.[3] (Fig. 2). Surface pressure orifices 0.025 in. in diameter were drilled from the airfoil surface into these six cavities. These orifices were located in chordwise planes at the 94.0, 96.6, 98.0, 98.7, 99.1, and 99.5% blade radius stations. In each plane, an orifice was located at the airfoil leading edge and 20 holes were located on both the upper and lower surfaces. The square, flat outboard tip was drilled with 25 pressure orifices, 9 of which were distributed along the chord line with the remaining 16 arranged symmetrically with respect to the chord line. Each cavity was fitted with a plug on which was cemented a Sensotec Type SA-8J-7F1 paddle-type pressure transducer. These transducers have an active 4-arm bridge bonded to a stainless steel diaphragm 1/8 in. in diameter, and have a nominal

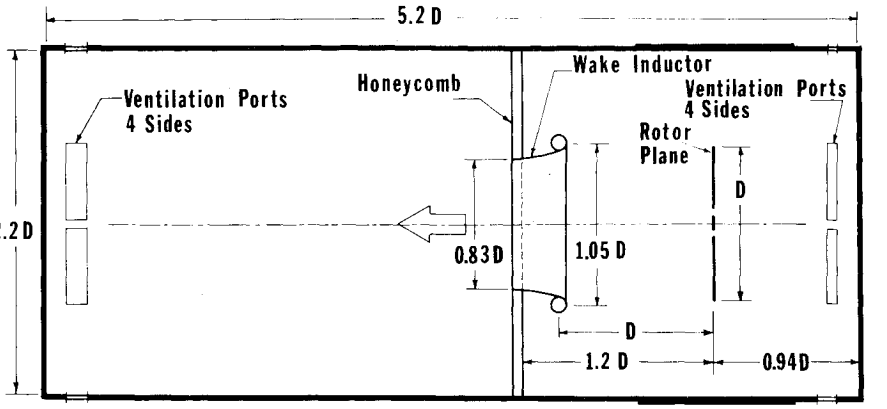

Fig. 1 Helicopter rotor test facility.

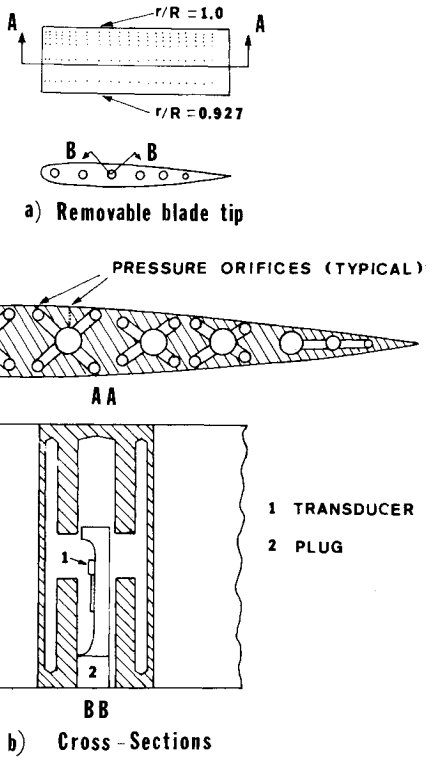

Fig. 2 Details of pressure tip design.

output of 3 mv/psi. Care was taken that the transducer diaphragms were all aligned perpendicular to the airfoil chord line so as to minimize the effect of inertial forces on the transducer output. The transducer wires were led along a tube inside the rotor blade to a terminal block on the rotor hub and then through mercury slip rings to a set of high-quality DC amplifiers. The signals were then routed through a scanner to an integrating digital voltmeter. Data acquisition was accomplished with a minicomputer.

Procedure

1. Static Calibration

An airtight box was installed over the end of the rotor blade and sealed at its inboard end with an O-ring around the blade contour. This box was pressurized with nitrogen and the box pressure was read on an electronic manometer, while the corresponding outputs of the six pressure transducers were read with the digital voltmeter. The static calibration was repeated at intervals during the data-taking period. The outputs of all transducers were linear with applied pressure and were repeatable within 1.5%.

2. Data Acquisition

Before a data run, the blade tip was covered with tape and then one orifice into each cavity was opened by piercing the appropriate hole with a needle. Thus, pressures were measured at six surface locations during each run. Preliminary tests with different tape orientations and thicknesses indicated that the measured pressures were not affected by the presence of the tape. Before starting a data run, a sample of six readings was taken from each transducer at 20-s intervals to establish the zero drift. An acceptable zero drift of the transducers was taken as a change, over an interval of 1 min, of less than 1% of the anticipated pressure levels. If the zero drifts were acceptable, the rotor was brought up to the desired rpm in less than 30 s and the outputs of the six transducers were measured and recorded. At least three readings were taken for each transducer over a time interval of 1 min. The rotor was then stopped in less than 20 s and the zero readings were repeated with sufficient samples to insure that an acceptable zero drift had been maintained. For all of these measurements, the digital voltmeter was set to integrate and average over 0.1 s. The value of each transducer output was determined by subtracting the initial zero reading from the first pressure measurement taken during the run and subtracting the final zero reading from the last pressure measurement taken; the average of the two differences represented the output. After correcting for acceleration effects (see subsection 3), the data were expressed in pressure-coefficient form by using the dynamic pressure corresponding to the ambient air density and the local blade velocity. The rotor tip was retaped after every run. Repeatability checks were routinely made in the course of filling out the pressure distribution data, and the repeatability of the data is shown in Figs. 3a and 4a. It is estimated that the uncertainty in the data presented is less than $\pm 5\%$, except for $X/C > 0.8$ where the uncertainty is less than $\pm 8\%$.

A Kulite-type CQL-080-5 transducer was mounted flush with the rotor surface at the 90.6% radial station and 7.5% chord station on the thrust side of the blade. This transducer was used in preliminary tests to confirm that the surface pressure on the rotating blade was essentially constant with time. Thus, the poor frequency-response characteristics inherent in mounting the transducers inside the cavities had a negligible effect on the surface pressure measurements.

3. Acceleration Correction

When diaphragm-type pressure transducers are installed in an accelerating system, the resulting inertial load on the diaphragm results in a diaphragm deflection and an output signal which is indistinguishable from that due to an applied pressure. In the present application, the centripetal acceleration of the rotor blade resulted in an inertial load of 1200 g at the transducer radial position at 1350 rpm. Although the transducers were carefully installed to insure that this load was tangential to the diaphragm and hence would have

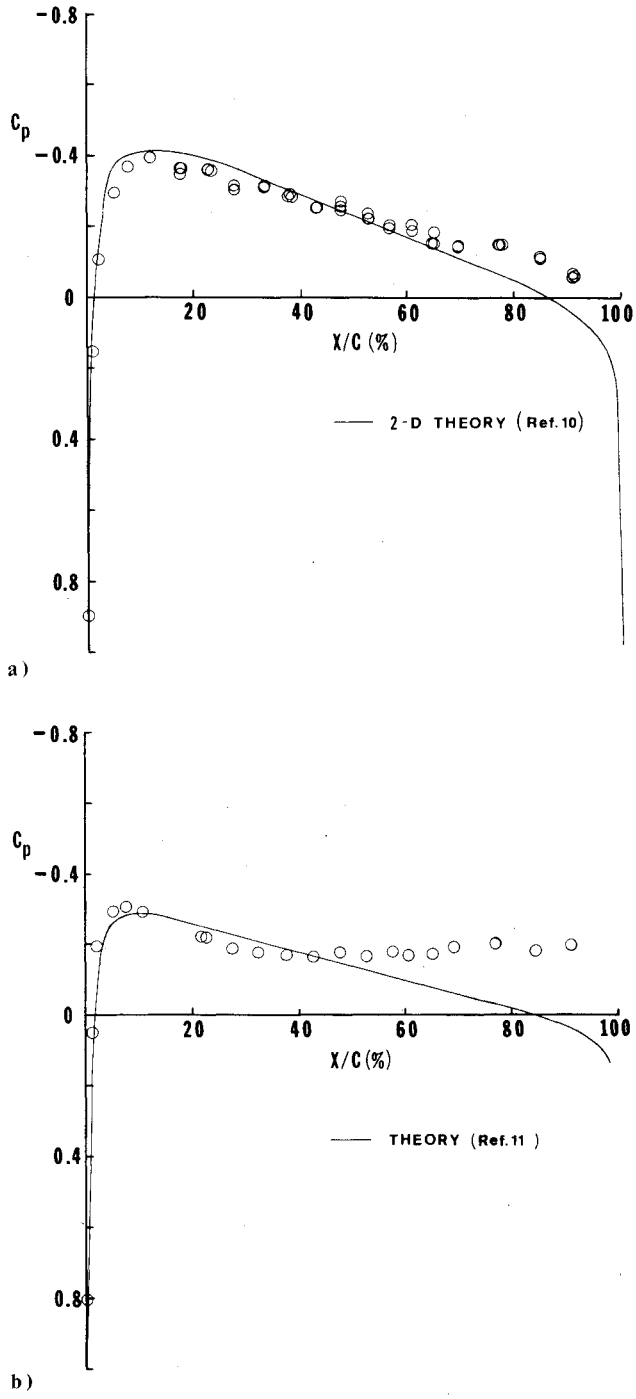

Fig. 3 Chordwise pressure distribution, $\theta = 0$ deg, 1350 rpm: a) $r/R = 0.940$, b) $r/R = 0.995$.

minimum effect, the "g" correction still was appreciable compared to the pressure signal. The correction was evaluated by carefully sealing all of the pressure orifices by first covering the blade surface with tape and then covering the tape with a stripable plastic-like paint. After taking transducer zeros, the blade was run up to operating rpm and the output of the six transducers was determined in the same manner as described earlier for obtaining pressure data. This measured transducer output was due to the inertial loading on the diaphragm and also on the column of air trapped in the cavity. The pressure change at the diaphragm, due to the inertial loading on the air column, was calculated for a given rpm, and the net transducer output after accounting for this effect represented the "g" correction which was applied to the data readings. The "g" correction was evaluated at $\theta = 0$ deg and was used to correct the data at all pitch angles. The effect, in fact, varies slightly with θ because of a small acceleration component normal to the diaphragm face, which is introduced because the transducers are not all at the one-quarter chord position and also because of coning of the blade during rotation. It was estimated that the variation of the correction with θ is so small as to be within the repeatability of the correction itself. The rotor blade is relatively heavy, so that the coning angle at maximum thrust is approximately 0.2 deg.

Pressure gradients due to the "g" effects on the air columns within the cavities also were accounted for in the data reduction if the orifice at which the pressure was being measured was at a different radial location than that of the transducer diaphragm.

Results and Discussion

Surface pressure measurements on the rotor near the tip ($r/R \geq 0.940$) were made at blade pitch angles, θ, of 0, 6.2, and 11.4 deg at a Reynolds number (based upon rotor tip speed and chord) of 7.36×10^5 (1350 rpm). A corresponding set of data was taken at a Reynolds number of 5.44×10^5 (1000 rpm) at $\theta = 0$ and 6.2 deg. These Reynolds numbers are considerably smaller than those encountered in full-scale helicopter rotor operation. However, the primary aim here is to provide data which can be used to suggest and evaluate analytical methods for calculating the aerodynamic loading on rotor blades.

Since, to the authors' knowledge, this is the first time that such detailed data have been available, the results for 1350 rpm are tabulated for reference in Tables 1-4. Each value in the tables represents the average of all the data taken at a particular location and test condition. The columns headed Row 1, Row 2, and Row 3 under "Flat Tip" refer to the pressures measured on the flat tip of the rotor. Row 1 is located 0.0375 chord lengths above the chord line of the symmetrical airfoil section; Row 2, along the chord line; and Row 3, 0.0375 chord lengths below the chord line.

Selected pressure distributions have been plotted in the figures. Figure 3 shows two chordwise pressure distributions at 0 deg pitch angle and 1350 rpm. At the innermost station ($r/R = 0.940$), the measured values agree well with conventional two-dimensional airfoil theory[10] over the first 50% of the chord. As one goes near the tip, the suction peak on the airfoil decreases because of a three-dimensional relief effect. At the outermost station ($r/R = 0.995$), the agreement with the semi-infinite wing theory of Raj[11] is good over the forward half of the surface. At both stations, the measured pressures are lower over the aft portions of the blade surface than those predicted by the theories. This is thought to be due to viscous effects and centrifugal pumping of the boundary layer, neither of which were taken into account in the theories.

The chordwise pressure distribution at three radial locations at a pitch angle of 6.2 deg and 1350 rpm is shown in Fig. 4. At the innermost station ($r/R = 0.940$), the measured pressures are compared with those predicted by the rotor blade element theory of Samant,[12] which takes account of inflow at the lifting line. It is seen that agreement is reasonable over the forward half of the airfoil. Again, the suction peak on the upper surface decreases toward the tip. The pressure level on the lower surface increases slowly with increasing radius. Outboard of $r/R = 0.980$ there is a second suction peak on the upper surface which is located near the trailing edge at $r/R = 0.987$, and which moves forward with increasing radius until it is at the 60% chord station at $r/R = 0.995$. This second peak is caused by the primary tip vortex. Because of the higher pressure on the underside of the rotor, the flow is around the tip and onto the upper surface. A vortex is formed and, coincident with its formation, local velocities are increased and the surface static pressures are decreased in the areas described.

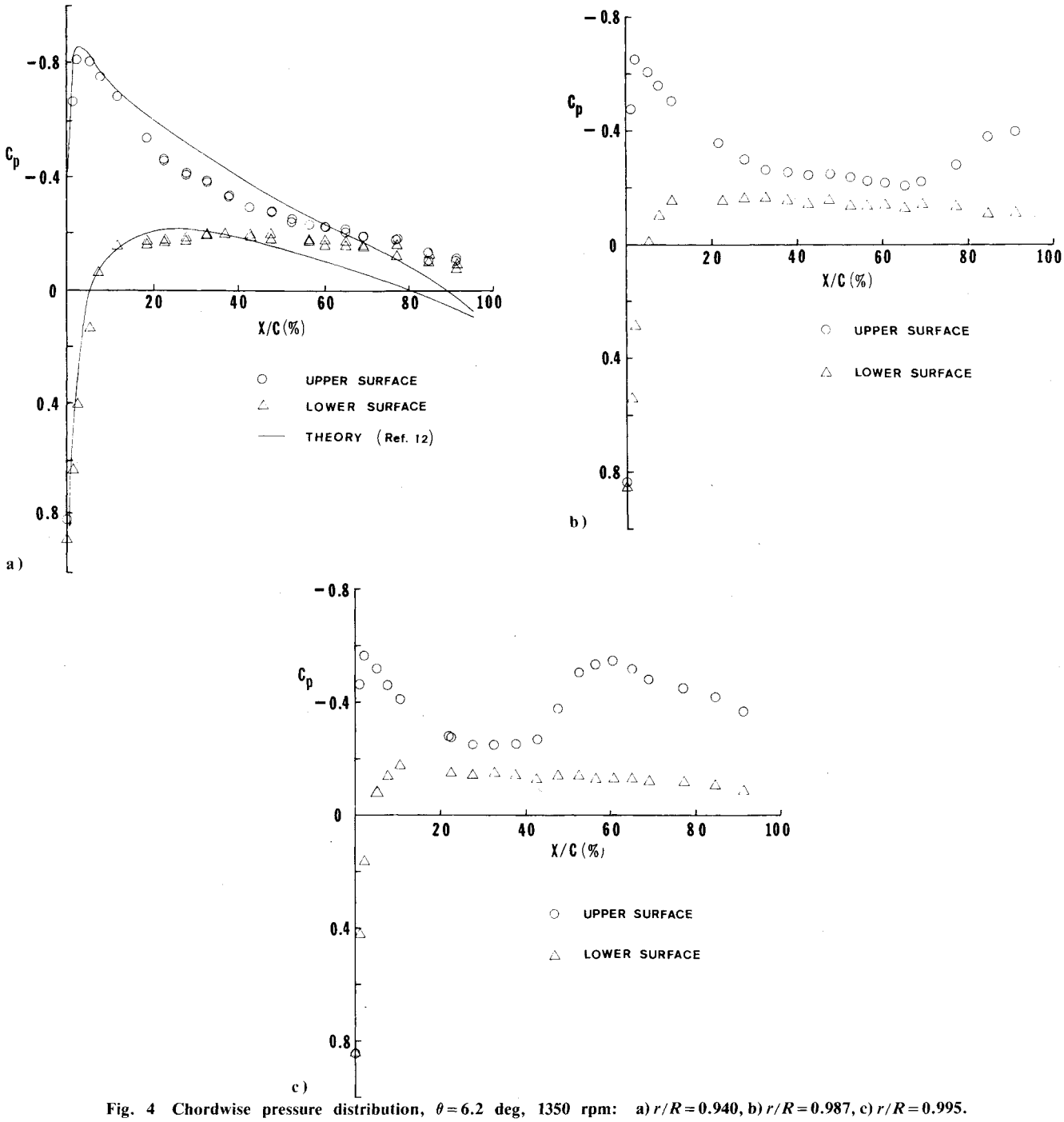

Fig. 4 Chordwise pressure distribution, $\theta = 6.2$ deg, 1350 rpm: a) $r/R = 0.940$, b) $r/R = 0.987$, c) $r/R = 0.995$.

Figure 5 shows a plot of lines of constant pressure on the upper surface of the rotor at a pitch angle of 6.2 deg. The values shown on the contours indicate pressure (psi) above or below ambient pressure. The isobar pattern indicates that the tip vortex is centered (i.e. has its maximum pressure effect) at about the 60% chord station at $r/R = 0.995$ and moves inboard and aft. This is also shown in the movement, with r/R, of the second suction peak in the chordwise pressure distributions (Fig. 4). The radial flow along the blade tip (from regions of high pressure to low pressure) is inboard over approximately the first 40% of the surface, outboard from about 40 to 75%, and then inboard again. These changes in radial flow direction are due to the presence of the tip vortex on the upper surface.

Figure 6 shows the chordwise pressure distribution at three radial stations at a pitch angle of 11.4 deg and 1350 rpm. At $r/R = 0.995$, there is seen to be a decrease in pressure aft of the second suction peak which was not present at $\theta = 11.4$ deg. It is thought that a small secondary vortex located very near the tip and centered near the trailing edge (about 73% chord) is associated with this pressure decrease (see Fig. 7, reproduced from Ref. 7). When these chordwise pressure distributions are compared with those of $\theta = 6.2$ deg, it is observed that the primary vortex moves toward the rotor leading edge with increasing pitch angle.

Constant pressure contours on the upper surface of the blade at $\theta = 11.4$ deg are shown in Fig. 8. The primary vortex is seen to be centered at about the 45% chord station at $r/R = 0.995$ and sweeps inboard and aft, as was the case at $\theta = 6.2$ deg. The same flow direction pattern is observed at $\theta = 11.4$ deg as at $\theta = 6.2$ deg. At $\theta = 11.4$ deg, the flow on the upper surface is inboard from the leading edge to about 30% chord, outboard from there to about 70% chord, and then inboard again.

Table 1 Pressure coefficient distribution on upper surface and flat tip, $\theta = 0$ deg, 1350 rpm

	Radial positions						Flat tip		
Chord, %	0.940	0.966	0.980	0.987	0.991	0.995	Row 1	Row 2	Row 3
.0	.897	.891	.875	861	.867	.809			
1.0	.157	.079	.097	.072	.080	.051			
2.0	−.104	−.098	−.153	−.179	−.151	−.193		−.461	
5.0	−.295	−.299	−.288	−.292	−.291	−.292			
7.5	−.368	−.351	−.340		−.305	−.305		−.158	
10.5				−.327	−.298	−.292			
11.5	−.390	−.365	−.347				−.329		−.338
18.5	−.362	−.344	−.293				−.194		−.150
21.5				−.278	−.244	−.219			
22.5	−.358	−.336	−.306	−.261	−.236	−.220		−.075	
27.5	−.313	−.296	−.240	−.217	−.205	−.186	−.110		−.085
32.5	−.309	−.261	−.230	−.207	−.197	−.175	−.072		−.068
37.5	−.287	−.250	−.218	−.214	−.194	−.170		−.044	
42.5	−.256	−.235	−.210	−.192	−.193	−.165	−.062		−.066
47.5	−.256	−.236	−.219	−.193	−.176	−.178	−.076		−.082
52.5	−.233	−.220	−.178	−.176	−.173	−.163		−.089	
56.5	−.200	−.193	−.153	−.161	−.154	−.178	−.080		−.088
60.5	−.196	−.172	−.152	−.149	−.157	−.167	−.108		−.112
65.0	−.172	−.155	−.145	−.144	−.160	−.170		−.095	
69.0	−.143	−.121	−.135	−.131	−.150	−.190			
77.0	−.150	−.151	−.162	−.145	−.187	−.197		.140	
84.4	−.113	−.130	−.129	−.145	−.160	−.182		−.115	
91.0	−.069	−.116	−.100	−.130	−.163	−.197		−.089	
93.0								.113	

Table 2 Pressure coefficient distribution on upper surface and flat tip, $\theta = 6.2$ deg, 1350 rpm

	Radial positions						Flat Tip		
Chord, %	0.940	0.966	0.980	0.987	0.991	0.995	Row 1	Row 2	Row 3
.0	.807	.812	.836	.835	.868	.849			
1.0	−.665	−.650	−.596	−.475	−.438	−.460			
2.0	−.812	−.734	−.722	−.652	−.593	−.561		−.621	
5.0	−.806	−.715	−.639	−.607	−.559	−.517			
7.5	−.752	−.680	−.613	−.560	−.513	−.460		−.178	
10.5				−.504	−.459	−.408			
11.5	−.685	−.615	−.539				−.188		−.442
18.5	−.535	−.468	−.415				−.126		−.280
21.5				−.359	−.330	−.284			
22.5	−.472	−.444	−.396	−.364	−.315	−.276		−.088	
27.5	−.412	−.380	−.320	−.300	−.266	−.247	−.134		−.227
32.5	−.385	−.310	−.269	−.264	−.247	−.249	−.114		−.198
37.5	−.334	−.267	−.262	−.254	−.241	−.250		−.064	
42.5	−.293	−.271	−.250	−.245	−.245	−.266	−.145		−.133
47.5	−.276	−.262	−.246	−.248	−.251	−.375	−.145		−.134
52.5	−.249	−.231	−.239	−.239	−.263	−.502		−.167	
56.5	−.233	−.220	−.218	−.225	−.287	−.532	−.180		−.120
60.5	−.226	−.216	−.203	−.218	−.331	−.548	−.201		−.131
65.0	−.211	−.202	−.200	−.205	−.382	−.516		−.190	
69.0	−.193	−.178	−.203	−.222	−.444	−.479			
77.0	−.183	−.162	−.182	−.280	−.461	−.448		−.185	
84.4	−.121	−.133	−.176	−.379	−.455	−.416		−.174	
91.0	−.109	−.119	−.149	−.395	−.421	−.365		−.157	
93.0								.123	

The chordwise pressure distributions taken at 1000 rpm were almost identical to those at 1350 rpm. The chordwise location of the suction peaks was unchanged and the chordwise pressure distributions indicated only minor variations which were within the error in measurement. Thus, the changes over the corresponding range of Reynolds number for $\theta = 0$ and 6.2 deg were small.

The pressure data discussed in the preceding paragraphs were examined and the results compared with flow visualization studies[2] made very near the tip of a rotor blade. The flow visualization techniques which were employed gave an indication of local flow direction and showed the presence of vortices on the upper surface of the rotor near the tip and also on the flat end of the blade. The surface flow directions inferred from the pressure contours (Figs. 5 and 8) agree with the flow directions observed in Ref. 2. The first point along the chord at which the radial flow near the blade tip suddenly changes direction was attributed in Ref. 2 to the inception of the tip vortex. The points of vortex inception in the pressure distributions (interpreted in the constant pressure contours as being the chordwise location at $r/R = 0.995$ where the radial pressure gradient changes sign) agree with those observed by flow visualization[2] and the same trend with increasing pitch angle is noted. At $\theta = 6.2$ deg, the pressure data indicate

Table 3 Pressure coefficient distribution on lower surface, $\theta = 11.4$ deg, 1350 rpm

	Radial Positions					
Chord, %	0.940	0.966	0.980	0.987	0.991	0.995
.0	.887	.862	.847	.861	.867	.845
1.0	.630	.626	.549	.543	.502	.426
2.0	.398	.380	.314	.287	.216	.165
5.0	.132	.029	−.014	−.010	−.038	−.079
7.5	−.064	−.088	−.097	−.098	−.104	−.133
10.5				−.153	−.144	−.175
11.5	−.158	−.154	−.162			
18.5	−.170	−.173	−.172			
21.5				−.162	−.149	−.152
22.5	−.173	−.181	−.181	−.150	−.159	−.149
27.5	−.180	−.180	−.179	−.162	−.151	−.138
32.5	−.200	−.191	−.178	−.162	−.154	−.147
37.5	−.202	−.185	−.171	−.154	−.145	−.139
42.5	−.191	−.169	−.162	−.140	−.140	−.127
47.5	−.191	−.179	−.162	−.154	−.147	−.138
52.5		−.169	−.158	−.132	−.134	−.136
56.5	−.174	−.159	−.153	−.134	−.139	−.126
60.5	−.168	−.164	−.121	−.139	−.135	−.129
65.0	−.167	−.154	−.145	−.123	−.134	−.125
69.0	−.159	−.145	−.139	−.124	−.126	−.117
77.0	−.145	−.148	−.145	−.132	−.122	−.117
84.4	−.134	−.133	−.129	−.109	−.104	−.104
91.0	−.088	−.106	−.122	−.109	−.109	−.084

Table 4 Pressure coefficient distribution on upper and lower surfaces, $\theta = 11.4$ deg, 1350 rpm

	Radial Positions						
	0.995		0.991	0.987	0.980	0.966	0.940
Chord, %	Upper surface	Lower surface	Upper surface	Upper surface	Upper surface	Upper surface	Upper surface
0	0.641		0.619	0.514	0.108		
1.0	−0.864	0.667	−0.937	−1.023	−1.180		
2.0	−0.917	0.356	−1.001	−1.126	−0.979	−1.329	−1.013
5.0	−0.694	−0.050	−0.804				−1.228
7.5	−0.634		−0.720	−0.796	−0.758	−0.796	
10.5	−0.505		−0.590	−0.657			
11.5						−0.794	−0.879
18.5					−0.458	−0.516	−0.618
21.5	−0.404	−0.096	−0.400	−0.439			
22.5	−0.411	−0.107	−0.390	−0.424	−0.390	−0.514	−0.484
27.5	−0.377	−0.125	−0.357	−0.360	−0.365	−0.407	−0.480
32.5	−0.465	−0.120	−0.338	−0.340	−0.340	−0.337	−0.435
37.5	−0.624	−0.119	−0.353	−0.345	−0.328	−0.340	
42.5	−0.735	−0.111	−0.379	−0.322	−0.323	−0.320	−0.333
47.5	−0.767	−0.169	−0.484	−0.362	−0.328	−0.351	−0.320
52.5	−0.648	−0.159	−0.608	−0.401	−0.308	−0.308	−0.332
56.5	−0.568	−0.180	−0.715	−0.446	−0.314	−0.293	−0.316
60.5	−0.590	−0.113	−0.701	−0.451	−0.277	−0.260	−0.243
65.0	−0.576	−0.116	−0.674	−0.506	−0.286	−0.242	−0.220
69.0	−0.606	−0.108	−0.695	−0.589	−0.275	−0.218	−0.197
77.0	−0.593	−0.099	−0.683	−0.691	−0.338	−0.185	−0.155
84.4	−0.581	−0.124	−0.648	−0.766	−0.413	−0.153	−0.139
91.0	−0.466	−0.069	−0.565	−0.704	−0.466	−0.132	−0.069

Table 5 Normal and chordwise force coefficients

	r/R	0.940	0.966	0.980	0.987	0.991	0.995
$\theta = 0.0$ deg	c_c	0.0142	0.0113	0.0130	0.0135	0.0174	0.0178
$\theta = 6.2$ deg	c_c	0.0059	0.0071	0.0094	0.0190	0.0238	0.0249
	c_n	0.198	0.167	0.160	0.217	0.245	0.276
$\theta = 11.4$ deg	c_c						0.0230
	c_n						0.471

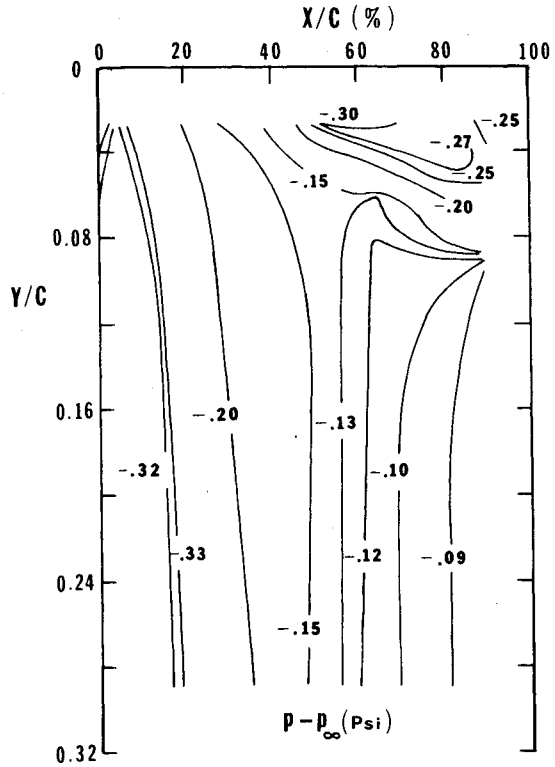

Fig. 5 Constant pressure contours upper surface, $\theta = 6.2$ deg, 1350 rpm.

vortex inception at 40% chord, while the results presented in Ref. 2 show the point of vortex inception to be at about the 44% chord station. At $\theta = 11.4$ deg, the present pressure data indicate vortex inception at the 28% chord station, while flow visualization[2] gives the 33% chord station.

The surface pressure measurements reported here were also compared with measurements made near the tip of a fixed wing.[7-9] The wing surface pressure measurements, which were on an NACA 0015 profile, indicated the presence of a primary and secondary vortex near the tip at an angle of attack of 12 deg; the same phenomena were observed in the present rotor tests for an NACA 0012 profile at a pitch angle of 11.4 deg. However, in the present case of the rotating blade, the primary suction peak is further along the chord than that measured for the fixed wing and the primary vortex is further outboard on the rotor than it is for the fixed wing.

Table 5 shows the normal and chordwise force coefficients obtained by integrating the pressure data at each of the six radial stations. The usual problems that arise in the determination of these coefficients are present here. These involve both the magnitude and location of the maximum and minimum pressure near the leading edge and the pressure distribution over the aft 9% of the section. Such data deficiencies are inherent in the method and are due to the physical limitations that arise in locating pressure taps. Thus, the pressure plots for the upper and lower surfaces at each station were extrapolated to a locally common pressure at the trailing edge and the data near the leading edge were faired to give what appeared to be reasonable maximum and minimum values. It is estimated that the normal force coefficients may be in error by approximately $\pm 1\%$ and the chordwise force coefficients by approximately $\pm 5\%$ as a result of these fairings and extrapolations.

Because of the rapid rise in the values of these coefficients very near the tip, it is apparent that the presently accepted tip loss corrections and models used in performance and blade stress calculations are not as appropriate as they have been thought to be. While a preliminary analysis appears to show that the effect on thrust for performance is merely a

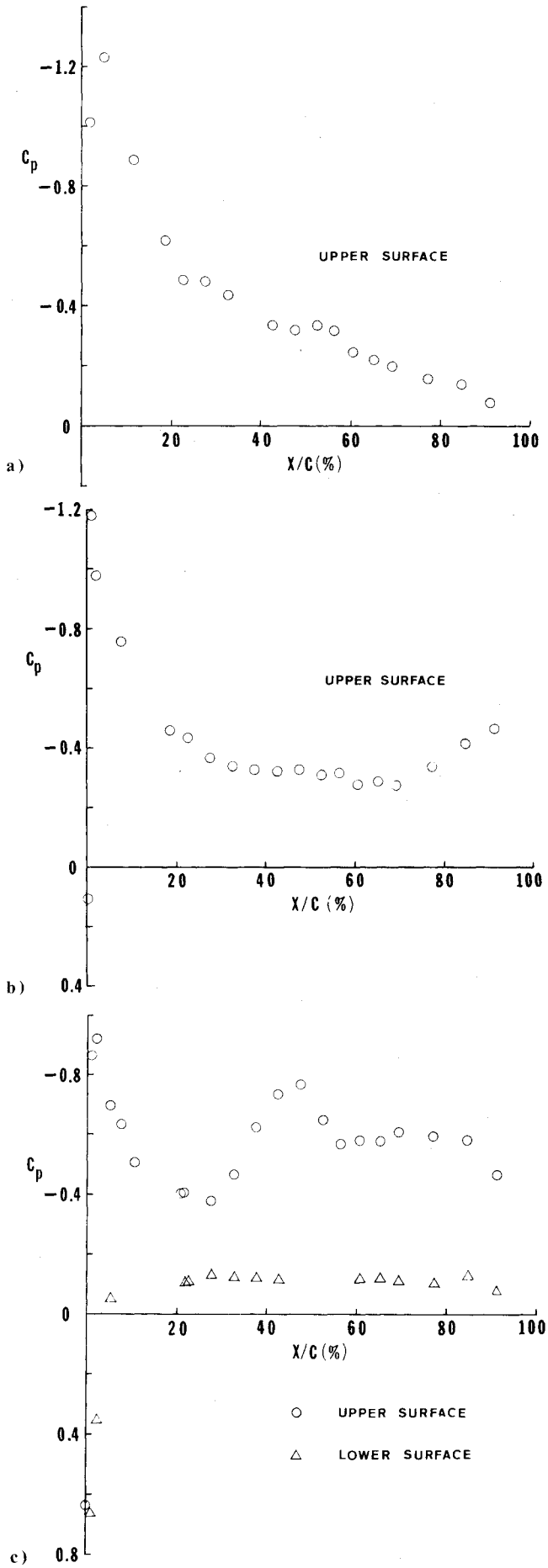

Fig. 6 Chordwise pressure distribution, $\theta = 11.4$ deg, 1350 rpm: a) $r/R = 0.940$, b) $r/R = 0.980$; c) $r/R = 0.995$.

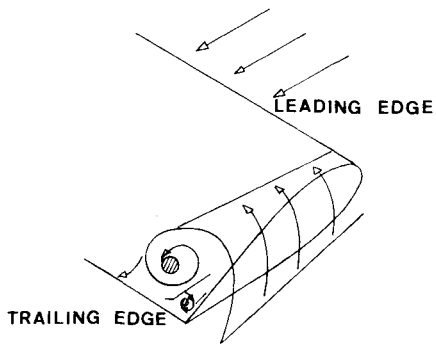

Fig. 7 Tip vortex schematic.

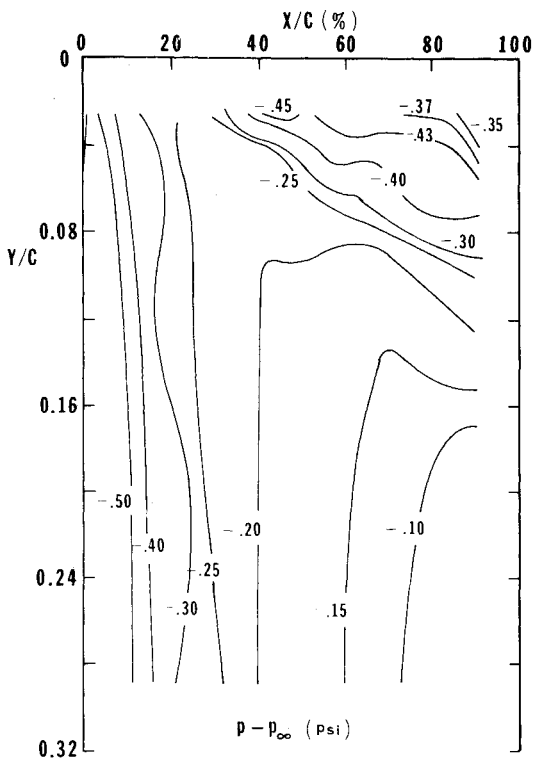

Fig. 8 Constant pressure contours upper surface, $\theta = 11.4$ deg, 1350 rpm.

redistribution of the loading near the tip in comparison to that calculated, it is not clear that a similar conclusion can be made for the torque loading since the equivalent high-drag coefficients occur at maximum dynamic pressure and radius.

Conclusions

The detailed surface pressure distribution data, taken at the tip of a single-blade helicopter rotor in hover, indicate the presence of a primary tip vortex on the upper surface which is centered at about the 60% chord station at a collective pitch angle of 6.2 deg. The vortex sweeps inboard and aft. With increasing pitch angle, the primary vortex moves toward the leading edge of the rotor.

At a pitch angle of 11.4 deg, the data indicate the presence of a small secondary vortex on the upper surface located very near the tip and near the trailing edge (about 73% chord). This secondary vortex has also been observed near the tip of a fixed wing at high angle of attack.

The points of vortex inception inferred from the pressure data are in satisfactory agreement with those noted by other investigators using surface flow visualization techniques.

The normal and chordwise force coefficients that were obtained by integrating the pressure data show a rapid rise in the values of both coefficients very near the tip. This behavior is very much different from the presently accepted tip loss correction models.

Acknowledgments

This work was supported in part by the U.S. Army Research Office under Grants DA-ARO-D-31-124-73-G184 and DAAG29-76-G-0007. R. Singleton of ARO was the technical monitor. The authors gratefully acknowledge the assistance of J. Craig in the development of the computer software, J. Caudell in the installation and checkout of the instrumentation, and J. Palfery in the design of the rotor.

References

[1] Ham, N.D., "Technical Evaluation Report on Fluid Dynamics Specialists' Meeting on the Aerodynamics of Rotary Wings," AGARD-AR-61, March 1973.

[2] Hoffman, J.D. and Velkoff, H.R., "Vortex Flow Over Helicopter Rotor Tips," *Journal of Aircraft,* Vol. 8, Sept. 1971, pp. 739-740.

[3] White, R.P. and Balcerk, J.C., "The Nemesis of the Trailed Tip Vortex – Is It Now Conquered?" Preprint No. 624, 28th Annual National Forum of the American Helicopter Society, Washington, D.C., May 1972.

[4] Scheimann, J. and Ludi, L.H., "Qualitative Evaluation of the Effect of Helicopter Rotor Blade Tip Vortex on Blade Airloads," NASA TN D-1637, May 1963.

[5] McCormick, B.W. and Surendraiah, M., "A Study of Rotor Blade-Vortex Interaction," Preprint No. 421, 26th Annual National Forum of the American Helicopter Society, Washington, D.C., June 1970.

[6] Spivey, W.A. and Morehouse, G.A., "New Insights into Design of Swept-tip Rotors," Preprint No. 420, 26th Annual National Forum of the American Helicopter Society, Washington, D.C., June 1970.

[7] Spivey, R.F., "Blade Tip Aerodynamics-Profile and Planform Effects," Preprint No. 205, 24th Annual National Forum of the American Helicopter Society, Washington, D.C., May 1968.

[8] Chigier, N.A., "Experimental Studies of Turbulent Aircraft Wakes," *Israel Journal of Technology,* Vol. 11, No. 6, pp. 367-372.

[9] Chigier, N.A. and Corriglia, V.R., "Tip Vortices-Velocity Distributions," Preprint No. 522, 27th Annual National Forum of the American Helicopter Society, Washington, D.C., May 1971.

[10] Abbot, I.A. and von Doenhoff, A.E., *Theory of Wing Sections,* Dover Publications, New York, 1959.

[11] Raj, P., "A Method of Computing the Potential Flow on Thick Wings Tips," Ph.D. Dissertation, School of Aerospace Engineering, Georgia Institute of Technology, Oct. 1976.

[12] Samant, S., "An Improved Method for Calculating the Tip Vortex Geometry for Hovering Rotors," Ph.D. Dissertation, School of Aerospace Engineering, Georgia Institute of Technology, Nov. 1976.